| 参赛学生姓名: | Yiran Zhu(朱一然) |
|---------------|---|
| | 上海外国语大学附属外国语学校 |
| | 上海市 |
| | 中国 |
| | <u>朱为宏</u> |
| | 华东理工大学 |
| | brication of a NTO/Ag/g-C ₃ N ₄ Self-supporting |
| | |
| | Efficient Photocatalytic Hydrogen Production |
| from Seawater | |

论文题目: Fabrication of a NTO/Ag/g-C₃N₄ Self-Supporting Membrane for Efficient Photocatalytic Hydrogen Production from Seawater

作者: Yiran Zhu (朱一然), 上海外国语大学附属外国语学校

Abstract

Hydrogen is now a key focus in clean energy. Splitting seawater under sunlight to produce hydrogen by photocatalytic technology, which converts solar energy to hydrogen energy, is an absolute green hydrogen technology. This study prepared a Z-scheme ternary composite catalyst by loading Ag nanoparticles on sodium titanate (Na₂Ti₃O₇, NTO) nanowires and compounding NTO with graphite phase carbon nitride (g-C₃N₄) semiconductors to form heterojunctions. The catalyst was further fabricated to a self-supporting membrane, which can not only prevent additional pollution of the powder catalyst to the ocean, but also made the catalyst recycle easy.

g-C₃N₄ was dissolved in the NTO/Ag solution, followed by a hydrothermal reaction at 130 °C for 24 h to prepare $TiO_2/Ag/g-C_3N_4$. The hydrogen production efficiency of the $TiO_2/Ag(2\%)/g-C_3N_4$ powder under visible light is approximately 365 μ mol/(g·h). The short nanorods structure of $TiO_2/Ag/g-C_3N_4$ makes it difficult to fabricate a self-supporting membrane of $TiO_2/Ag/g-C_3N_4$.

P25 powder, Ag nanoparticles and g-C₃N₄ were added to a strongly alkaline NaOH solution, followed by a hydrothermal reaction at 130 °C for 24 h to prepare NTO/Ag/g-C₃N₄. The hydrogen production efficiency of the NTO/Ag(2%)/g-C₃N₄ powder under visible light is approximately 660 μmol/(g·h), and the hydrogen production efficiency of the NTO/Ag(5%)/g-C₃N₄ powder reaches 1168 μmol/(g·h), both of which are much higher than that of the TiO₂/Ag(2%)/g-C₃N₄ powder, and the catalytic efficiency increases with the increase of the Ag content. After suction filtration and freeze-drying, a self-supporting membrane of NTO/Ag/g-C₃N₄ with good performance was prepared. After the 3-h hydrogen production reaction, the self-supporting membrane still maintains its original morphology, without hydrolysis or decomposition, so that the catalyst can be conveniently recycled.

The enhancement of the photocatalytic performance of NTO/Ag/g-C₃N₄ is mainly attributed to the construction of the Z-scheme multi-dimensional heterostructure, while zero-dimensional Ag nanoparticles decorated on the surface of NTO nanowires not only act as electron mediator for the formation of Z-scheme between NTO and g-C₃N₄, but also provide hot electrons due to their plasma effect. g-C₃N₄ is non-toxic, environmentally friendly, and with high visible light response capability, which can improve both the visible light absorption range and intensity.

Key words: NTO/Ag/g-C₃N₄, Splitting Seawater, Hydrogen Production, Photocatalysis, Self-Supporting Membrane

Contents

Abstract

| 1、 | Introduction | | 1 |
|----|------------------|---|----|
| | 1.1 | Background | 1 |
| | 1.2 | Research Status | 1 |
| | 1.3 | Objectives and Innovations | 5 |
| 2、 | Exper | imental | 7 |
| | 2.1 | Preparation of Ag Nanoparticles | 7 |
| | 2.2 | Preparation of Sodium Titanate Nanowires (Na ₂ Ti ₃ O ₇ , NTO) | 7 |
| | 2.3 | Preparation of NTO/Ag | 8 |
| | 2.4 | Preparation of TiO ₂ /Ag(2%)/g-C ₃ N ₄ | 8 |
| | 2.5 | Preparation of NTO/Ag/g-C ₃ N ₄ | 9 |
| | 2.6 | Preparation of Self-Supporting Membranes of Ternary Composite Catalysts | 9 |
| | 2.7 | Characterization of Photocatalysts | 10 |
| | 2.8 | Visible Light-Driven Hydrogen Production by Simulated Seawater Splitting | 10 |
| 3、 | Resul | ts and Discussion | 13 |
| | 3.1 | Characterization of Photocatalysts | 13 |
| | 3.2 | Visible Light Absorption Analysis | 18 |
| | 3.3 | Membranes Fabrication | 20 |
| | 3.4 | Hydrogen Production by Photocatalytic Seawater Splitting | 22 |
| | 3.5 | Mechanism of NTO/Ag/g-C ₃ N ₄ for photocatalytic Hydrogen Production | 25 |
| 4、 | Conc | lusions and Outlooks | 27 |
| | 4.1 (| Conclusions | 27 |
| | 4.2 (| Outlooks | 28 |
| Re | References | | |
| Ac | cknowledgements3 | | |

1. Introduction

1.1 Background

Hydrogen, whose combustion produces only water, has now become a focal point of global clean energy research. However, commonly used industrial hydrogen production methods, such as water electrolysis, natural gas reforming, and methanol reformation, are energy-intensive and emit significant amounts of carbon dioxide. Developing clean and pollution-free methods for hydrogen production is now the main focus.

On the other hand, our planet holds vast, inexhaustible resources in the form of solar energy and seawater. Using photocatalytic technology, seawater can be split into hydrogen under sunlight in an environmentally friendly and pollution-free process, which qualifies as an entirely "green hydrogen" production method.

This study designed and fabricated a photocatalyst membrane. When this catalyst membrane is immersed in the seawater like a fishing net used by fishermen, it can split seawater to produce hydrogen under sunlight irradiation. After the reaction is completed, the membrane can be "retrieved like a net"—without causing additional pollution to seawater, as shown in Fig. 1.1.



Fig. 1.1 Hydrogen harvesting from sea

1.2 Research Status

In 1972, Akira Fujishima and co-researchers from Japan first discovered that a titanium dioxide (TiO₂) single-crystal electrode could split water into hydrogen under

light, enabling the direct conversion of solar energy into chemical energy [1]. This breakthrough garnered significant attention for photocatalysis technology. The mechanism of photocatalysis using semiconductor catalysts is shown in Fig. 1.2.

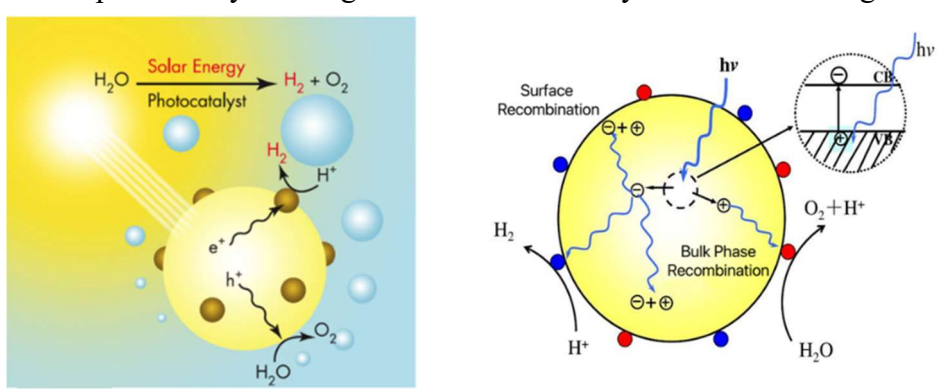


Fig. 1.2 Mechanism of Semiconductor Photocatalysis [2]

The semiconductor material absorbs photons and excites electrons from the valence band to the conduction band to generate photogenerated electrons when it is exposed to light with energy equal to or greater than its band gap. Simultaneously, positively charged holes are left in the valence band, forming electron-hole pairs. The photogenerated electron-hole pairs migrate to the semiconductor surface under an electric field or concentration gradient. During migration, some electron-hole pairs recombine, releasing energy as heat or light, which reduces photocatalytic efficiency. Successfully migrated electron-hole pairs on the semiconductor surface participate in chemical reactions [3-6].

TiO₂, with its suitable band structure, chemical stability, non-toxicity, and low cost, is the most commonly used photocatalyst. Titanate-titanium containing oxysalt- share a structural similarity with TiO₂ and can convert into compact TiO₂, enabling uniform doping or molecular assembly ^[7].

However, the solar-driven hydrogen production efficiency of TiO₂ and titanates remains low due to their wide band gap (3.0–3.2 eV), which only absorbs about 5% of total solar energy in the ultraviolet region. Additionally, photogenerated electron-hole pairs in TiO₂ is easy to recombine, further limiting photocatalytic efficiency. To address these challenges, researchers have explored strategies such as noble metal doping, nano structuring, and heterojunction construction ^[8].

1. Precious metal doping

Enhancing visible light absorption and photocatalytic activity by modifying Tibased photocatalysts with precious metals like Pt and Ag is a common approach ^[9-12]. For example, Liu ^[13] achieved a band gap reduction from 3.21 eV to 3.09 eV by loading Au nanoparticles on TiO₂ hollow microspheres (THMs). Dong ^[14] significantly improved the hydrogen production performance of GaN by Pt nanoclusters precipitation on nanowires. Dae-Hyeong Kim ^[15] designed a floating photocatalytic platform composed of a porous elastomer-hydrogel nanocomposite. The nanocomposite at the air-water interface had efficient light transmission, and the metalloaded Pt/TiO₂ and Cu/TiO₂ photocatalysts both showed high hydrogen evolution efficiency.

2. Nanostructure and morphology control of TiO₂

Developments in nanotechnology have enabled precise control of the morphology of TiO₂, significantly increasing surface area and improving charge transport properties. One-dimensional nanostructures such as nanotubes and nanorods exhibit superior charge separation and transfer efficiency. Emerging two-dimensional TiO₂ nanosheets further offer enhanced surface-active sites and shortened charge transfer distances. Li reviewed the development of nanostructured TiO₂ (including nanotubes, nanorods and 2D materials) for efficient hydrogen production, focusing on improving charge separation and increasing active surface area ^[16]. Guo ^[17] prepared WSe₂/TiO₂ nanocomposites via a mechanical grinding method. The heterojunction formed between TiO₂ and WSe₂ nanosheets facilitated the interfacial charge separation, thereby enhancing the hydrogen production rate.

3. Heterojunction Construction

Constructing a heterojunction by combining narrow-bandgap semiconductors with Ti-based semiconductors is also a common method for enhancing visible light absorption efficiency. Narrow-bandgap semiconductors have strong absorption capacity for visible light. After coupled with Ti-based semiconductors to form a heterojunction, the light response range of Ti-based semiconductors can be effectively

expanded to the visible light region. The relative position of the conduction band and the valence band between the narrow-bandgap semiconductord and the Ti-based semiconductor determines the direction of charge transfer in the photocatalytic process. Photogenerated electrons and holes can be effectively separated between different components according to their energy band structure, thereby improving the photocatalytic activity [18]. Currently, the common types of heterojunctions include Type-II, Z-scheme, and S-scheme heterojunctions. The distinction among these three heterojunction types lies in the differences in their carrier migration pathways ^[19]. The catalytic mechanisms of different heterojunction types are illustrated in Fig. 1.3.

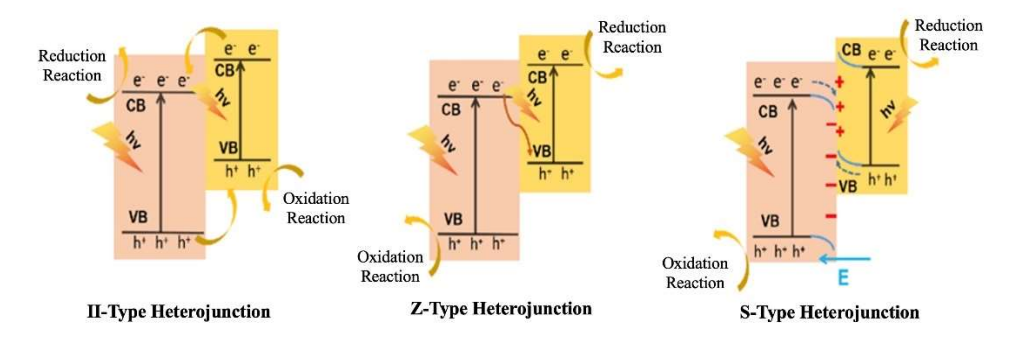


Fig. 1.3 Direction of charge transfer of three types of heterjunctions [20]

In order to maximize the catalytic performance of photocatalysts, it is of great significance to develop multi-component composite materials with different properties. The rational design of multi-component composite photocatalysis is conducive to the combination of multiple modification methods. At the same time, effective heterogeneous interface design can also promote the optimization of material performance. Li et al. [21] proposed a sandwich-structured CdS-Au-TiO₂ nanorod array as the photoanode in a photoelectrochemical cell for hydrogen production via water splitting. Firstly, the TiO₂ nanorod array was prepared on a fluorine-doped tin oxide (FTO) substrate by a hydrothermal method. Subsequently, the TiO₂ nanorod array was immersed in an aqueous HAuCl₄ solution for 4 h, and after annealing, an Au-modified TiO₂ nanorod array was obtained. Finally, CdS quantum dots were deposited on the surface of the Au-modified TiO₂ nanorod array through electroless plating deposition. In this structure, the Au nanoparticles sandwiched between the TiO₂ nanorods and the

CdS layer play a dual role in enhancing the solar-to-chemical energy conversion efficiency.

Most of the current Ti-based semiconductor catalysts are predominantly in powder form. Owing to the intrinsic high surface energy of nanoparticles, these powder catalysts are prone to agglomeration, which ultimately leads to the formation of a large amount of "dead volume" [22]. Under prolonged light irradiation, powder catalysts are susceptible to the effects of photocorrosion, redox cycling, and other factors, resulting in a significant attenuation of their long-term catalytic activity. Furthermore, such powder catalysts pose considerable challenges in recovery during practical application and are likely to induce secondary pollution.

In contrast to powder catalysts, self-supported catalysts exhibit distinct application advantages. From the perspective of micro-morphology, self-supported catalysts mostly present as ordered nanoarray structures, which can effectively accelerate the interfacial charge transfer kinetic process and significantly enhance the mechanical stability of the catalyst under long-term continuous operating conditions. In addition, leveraging flexible and tunable nanostructure design strategies, the catalytically active specific surface area of self-supported materials can be substantially increased—this characteristic is more conducive to exposing abundant catalytic active sites [23, 24]. More importantly, after the end of their service cycle, self-supported catalysts possess the property of convenient recovery and recycling, which can effectively avoid potential environmental pollution risks.

1.3 Objectives and Innovations

This study designed and fabricated a multi-dimensional NTO/Ag/g-C₃N₄ catalyst on the basis of sodium titanate (Na₂Ti₃O₇, NTO) ultra-long nanowires. Specifically, the one-dimensional NTO nanowires serve as a flexible matrix, the zero-dimensional Ag nanoparticles act as electron conductors to increase the number of active sites on the nanowire surface, and the two-dimensional g-C₃N₄ nanosheets form a heterojunction with NTO, which facilitates the efficient separation and rapid transfer of photogenerated carriers. A self-supporting membrane of the NTO/Ag/g-C₃N₄ catalyst

was prepared based on the flexible structure of the NTO ultra-long nanowires, which can not only enable green hydrogen production with high efficiency but also realize the recovery and reuse of the catalyst, avoiding environmental pollution caused by the catalyst.

2. Experimental

2.1 Preparation of Ag Nanoparticles

Ag nanoparticles were prepared by chemical reduction. Put 340 mg of silver nitrate (AgNO₃, Titan Technology Co., Ltd, China) and 333 mg of polyvinylpyrrolidone (PVP, Titan Technology Co., Ltd, China) into 10 mL of deionized water, disperse the solution evenly by ultrasonic dispersion for 5 min to obtain solution A. Dissolve 80 mg of sodium hydroxide (NaOH, 96%, Titan Technology Co., Ltd, China) and 18.9 mg of sodium borohydride (NaBH₄, 98%, Titan Technology Co., Ltd, China) in 10 mL of deionized water, which is dispersed by ultrasonic dispersion for 5 min to obtain mixed solution B. Place solution A in a constant temperature water bath at 45 °C and maintain a stirring speed of 400 rpm, slowly inject 10 mL of solution B into solution A by a syringe pump at a speed of 0.1 mL/min, ultrasonicate the resulting solution at room temperature for 1 h. The obtained solution was centrifuged and washed with deionized water until pH≈7. The final product (Ag nanoparticle suspension) was stored in a brown bottle. To standardize the concentration, 1 mL of the suspension was transferred into a centrifuge tube. The tube was weighed to record the mass, and then was placed in a vacuum dryer for 24 h, after which the mass of the dried Ag nanoparticles was recorded once more. From these measurements, the Ag concentration in the suspension (mg/mL) was determined.

In the above process, AgNO₃ provides Ag ⁺ ions, while NaBH₄ acts as a reducing agent to reduce Ag ⁺ ions to elemental Ag and form Ag particles. Polyvinylpyrrolidone (PVP) serves as a protective agent that wraps around the surface of Ag nanoparticles, preventing them from binding to each other and thus avoiding the aggregation and precipitation of Ag nanoparticles.

2.2 Preparation of Sodium Titanate Nanowires (Na₂Ti₃O₇, NTO)

This study fabricated NTO nanowires by hydrothermal reaction. Titanium dioxide (TiO₂, P25) nanoparticles are subjected to a series of chemical reactions under strong alkaline conditions and specific temperature and pressure, followed by proton exchange to yield nanowires. Typically, the nanowires obtained directly from the hydrothermal reaction are amorphous, thus, further acid washing is required to obtain NTO nanowires with photocatalytic activity and a stable morphology.

12 g of NaOH was dissolved in 30 mL of deionized water. Subsequently, 200 mg of P25 powder (Evonik Degussa (China) Co., Ltd) was added to the prepared NaOH solution. The resulting mixture was then transferred to a magnetic stirrer and stirred at a constant speed for 5 min to ensure uniform dispersion of P25 particles as Fig. 2.1. The well-dispersed suspension was then carefully transferred into a teflon-lined autoclave to initiate the hydrothermal reaction with the reaction temperature of 130 °C for 24 h. After reaction, the whole reaction system was cooled naturally to room temperature.





Fig. 2.1 P25 dissolved in NaOH

Fig. 2.2 Hydrothermal reaction system

Thereafter, the as-synthesized NTO suspension were subjected to washing with a 0.1 mol/L dilute hydrochloric acid (HCl) solution to remove residual NaOH and stabilize the nanowire structure. The product was then repeatedly rinsed with deionized water until the suspension reached neutrality(pH \approx 7). Finally, the neutralized product was transferred to a vacuum drying oven and dried at a predefined temperature for 12 h, yielding NTO powder with a well-defined structure.

2.3 Preparation of NTO/Ag

NTO/Ag was prepared by adding pre-prepared Ag nanoparticles into the reaction system of NTO. In this study, 4 mg of Ag nanoparticles (certain volume of Ag suspension) and 200 mg of P25 powder were added in 30 ml of NaOH (10 M) solution. Then the mixture was hydrothermal treated in a teflon-lined autoclave at 130 $^{\circ}$ C for 24 h with a stirring speed of 300 rpm. After reaction, the reaction products were then cooled to room temperature, centrifugally washed to neutrality, and vacuum dried.

2.4 Preparation of TiO₂/Ag(2%)/g-C₃N₄

30 mg of the pre-prepared NTO/Ag powder and 5 mg of g-C₃N₄ were dissolved in 30 mL of deionized water. After stirring for 30 min, the mixed solution was put in an

autoclave for hydrothermal reaction at the temperature of 130 °C for 24 h and the stirring speed at 300 rpm. After reaction, the product was cooled and centrifuged washed with deionized water to neutral. A part of the product was placed in a vacuum drying oven for 12 h to obtain ternary catalyst powder, while the remainder was reserved for the fabrication of self-supporting membrane experiment.

2.5 Preparation of NTO/Ag/g-C₃N₄

Dissolve P25 powder (200 mg), g-C₃N₄ (5 mg), NaOH (12g), and Ag nanoparticles (4 mg for NTO/Ag(2%)/ g-C₃N₄, 10 mg for NTO/Ag(5%)/ g-C₃N₄) in deionized water of 30ml. The mixed solution was then placed in a hydrothermal environment at 130 °C for 24 h with the stirring speed of 300 rpm. After reaction and cooling, wash the product to neutrality. Dry a portion to obtain NTO/Ag(2%)/ g-C₃N₄ and NTO/Ag(5%)/ g-C₃N₄ powder, while the rest is for suction filtration.

2.6 Preparation of Self-Supporting Membranes of Ternary Composite Catalysts

The suspension of TiO₂/Ag/g-C₃N₄ and NTO/Ag/g-C₃N₄ were slowly transferred into a suction filtration flask as Fig.2.3. The vacuum pump was activated to initiate suction filtration, and the process continued until no additional liquid efflux was observed, finally obtaining membranes with a diameter of approximately 30 mm, which were then subjected to vacuum drying and freeze drying respectively.



Fig. 2.3 Suction filtration system





Fig. 2.4 Vacuum drying oven and lyophilizer

2.7 Characterization of Photocatalysts

The crystal structure of the as-prepared samples were measured by the D8 Advance Powder X-ray Diffraction (XRD, Bruker, Germany) with Cu Ka radiation at 0.15418 nm. The morphology of the samples were examined by a field emission scanning electron microscope (SEM, Hitachi, Japan). Transmission electron microscopy (TEM) and energy dispersive X-ray analysis (EDX) of prepared photocatalysts were taken by Tecnai G2 F30 S-Twin transmission electron microscope (FEI, U.S.A) with an accelerating voltage of 300 kV. The UV-vis diffuse reflectance spectra (UV-vis-DRS) of the prepared catalysts over the range of 250-800 nm were obtained using a Lambda 700 UVeVis NIR spectrometer (PerkinElmer, U.S.A).

2.8 Visible Light-Driven Hydrogen Production by Simulated Seawater Splitting

The visible-light-driven photocatalytic splitting of simulated seawater to produce hydrogen was carried out in a quartz photoreactor. A Xenon lamp (PLS-SXE300, Prefect Light, China), employed as the simulated solar light source, was positioned 5 cm above the quartz photoreactor. An optical filter with a cutoff wavelength of $\lambda \ge 420$ nm was attached to the Xenon lamp to ensure that the transmitted light was predominantly in the visible region.

The quartz photoreactor was coupled to a closed gas circulation system. Throughout the entire experimental process, circulating water was continuously introduced into the system to maintain the photoreactor at ambient temperature. A gas chromatograph was utilized for periodic sampling and analysis of the gaseous products

in the photoreactor (GC7890A, Agilent, USA), with measurements performed at 30-min intervals. The system was first purged with nitrogen gas for 30 min under dark conditions to remove dissolved oxygen in the solution and the mixed gas in the photoreactor. Each photocatalytic reaction cycle lasted 3 h. The photocatalytic H₂ production system is illustrated in Fig. 2.5.

As the core light-emitting component in solar simulators, the Xenon lamp generates light via the ionization of high-pressure Xenon gas to form an electric arc. It exhibits a broad spectral range, spanning multiple wavelength bands from the ultraviolet (UV) to infrared (IR) regions, which demonstrates high similarity to the spectral profile of natural sunlight. Additionally, the Xenon lamp is characterized by high luminous intensity and high color temperature, enabling it to emit bright light that closely resembles natural sunlight. This unique combination of properties allows the Xenon lamp to provide sufficient light intensity for solar simulation while retaining a color temperature comparable to that of natural sunlight.

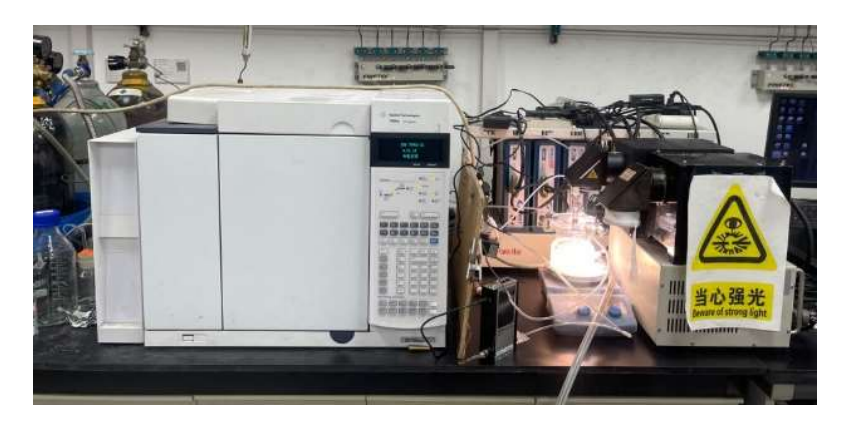


Fig. 2.5 Visible Light-Driven Hydrogen Production Setup

The component of the simulated seawater was as follows: NaCl (27.21 mg/mL), MgCl₂ (3.81 mg/mL), MgSO₄ (1.66 mg/mL), CaSO₄ (1.404 mg/mL), K₂SO₄ (0.577 mg/mL), K₂CO₃ (0.2124 mg/mL) and MgBr₂ (0.08 mg/mL). The salinity of the solution was 34.95‰, closely matching the global average seawater salinity of approximately 35‰. All the materials were supplied by Sinopharm Group Co., Ltd..

Hydrogen production experiments were conducted using different kinds of catalyst, NTO, NTO/Ag, TiO₂/Ag/g-C₃N₄ powders, NTO/Ag/g-C₃N₄ powders and NTO/Ag/g-C₃N₄ self-supporting membranes. For powder catalysts, the catalysts were ultrasonically dispersed in simulated seawater, stirred at 400 rpm to maintain suspension. For membrane catalysts, the membranes were directly immersed without ultrasonic dispersion.

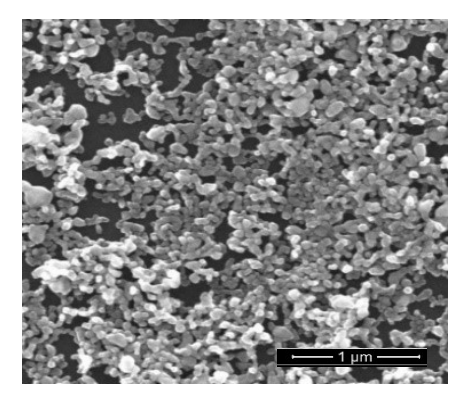
Sodium sulfide (Na₂S·9H₂O, Aladdin Biochemical Technology Co., Ltd., China) and sodium sulfite (Na₂SO₃, Aladdin Biochemical Technology Co., Ltd., China) were used as sacrificial agents to enhance hydrogen production efficiency by providing electrons, scavenging holes, and stabilizing the photocatalyst,

3、Results and Discussion

3.1 Characterization of Photocatalysts

The Ag particles and its morphology obtained by the chemical reduction are shown in Fig. 3.1. Ag nanoparticles prepared by chemical reduction are well dispersed with uniform grain size of approximately 18 nm.





(a) Ag suspension

(b) SEM of Ag Nps

Fig. 3.1 Ag particles obtained by the chemical reduction method

The SEM image of P25 powder is shown in Fig. 3.2(a). It is also uniformly sized and well-dispersed, with an average particle size of approximately 13 nm. After the hydrothermal reaction in the strong alkalinity NaOH solution for 24 h, P25 was transferred to NTO ultra-long nanowires. The NTO suspension obtained by the hydrothermal reaction appears to be a white flocculent mixture, as Fig. 3.2(b), which allows for the preliminary inference that substances with a linear structure have been formed.

Some studies suggest that the flocculent products prepared by the hydrothermal method form stable nanowire structures during the subsequent acid washing process. During the hydrothermal reaction, the Ti-O-Ti bonds of TiO₂ break and react with NaOH to form Ti-OH bonds and Ti-O-Na bonds. The Ti-O-Na bonds and Ti-OH bonds form new Ti-O-Ti bonds during the acid washing process, accompanied by the formation of fragments ^[25]. In the acid washing process, the Ti-OH bonds form Ti-O-H-O-Ti or Ti-O-Ti bonds through dehydration reactions, which shortens the bond length between Ti atoms on the surface. Eventually, the Ti-OH fragments bend and

connect with other fragments to form nanowires [25].

The morphology of NTO nanowires is shown as Fig. 3.2(d) and Fig. 3.2(e), with a length almost 10 µm and a diameter of approximately 30 to 50 nm. The NTO nanowires are intertwined with each other like "fibers", which can not only ensure outstanding catalytic performance, but also possess good mechanical properties such as strength and toughness to serves as the basis for preparation of the self-supporting membranes of the catalyst.

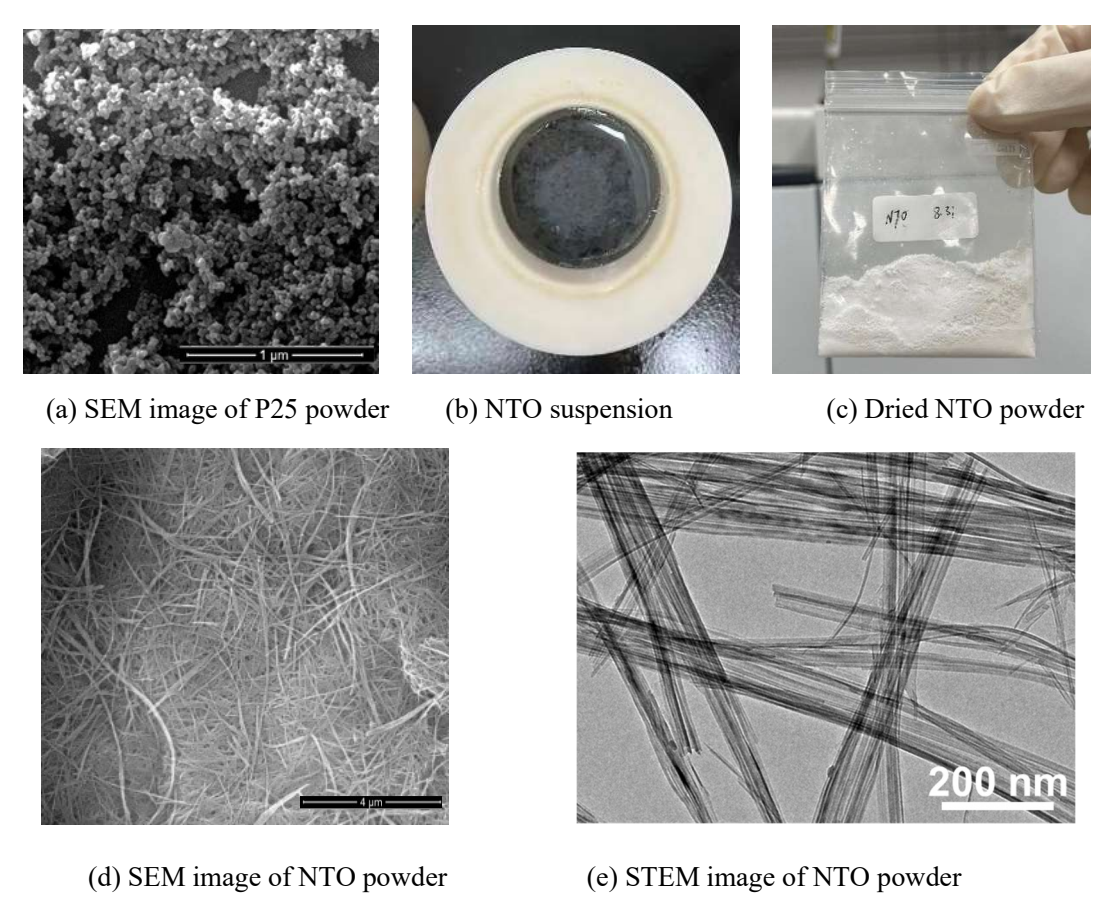
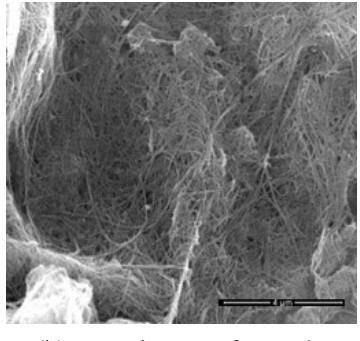
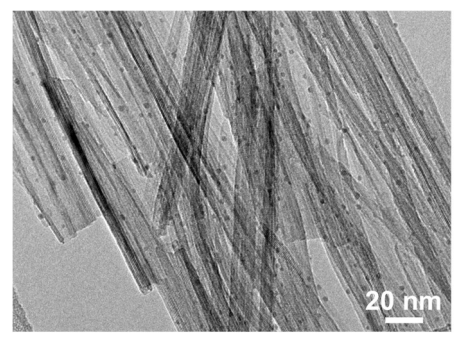


Fig. 3.2 Morphology of P25 and NTO

The as-prepared NTO/Ag powder is shown in Fig. 3.3(a). Obviously, the incorporation of Ag particles lead to a color transition of the powder—specifically, the originally white NTO powder was converted to brown NTO/Ag powder. As observed from the SEM and STEM images, the NTO loaded with Ag particles still maintains a nanowire structure, with the nanowires exhibiting more pronounced curling and entanglement. Additionally, Ag nanoparticles are uniformly attached to the surface of NTO nanowires.







(a) NTO/Ag powder

(b) SEM image of NTO/Ag

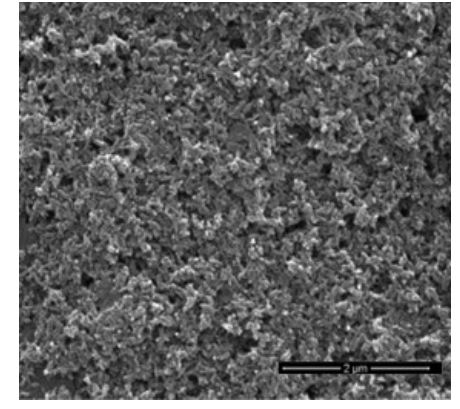
(c) STEM image of NTO/Ag

Fig. 3.3 NTO/Ag powder and its morphology

The NTO/Ag binary composite modifies the structure of NTO through the loading of Ag nanoparticles, which may enhance its visible-light absorption capacity and improve the catalytic performance of NTO.

The suspension of TiO₂/Ag/g-C₃N₄ by mixing the as-prepared NTO/Ag powder and g-C₃N₄ powder in the deionized water to hydrothermal react is shown as Fig. 3.4(a), which shows that the solid product is in the form of dispersed particles, and the ultralong nanowires of NTO formed in the previous hydrothermal reaction disappears. The SEM image (Fig. 3.4(b)) shows that a large number of rod-shaped TiO₂/Ag particles are loaded on the uniformly dispersed flake-like g-C₃N₄, which is because the NTO nanowires generated in the previous hydrothermal reaction underwent hydrolysis and transformed into short rod-shaped TiO₂ during the last hydrothermal reaction. The preparation of the TiO₂/Ag/g-C₃N₄ ternary composite material by two-step hydrothermal reaction is shown in Fig. 3.5.





(a) Suspension of TiO₂/Ag/g-C₃N₄

(b) SEM image of TiO₂/Ag/g-C₃N₄

Fig.3.4 TiO₂/Ag/g-C₃N₄ suspension and SEM images

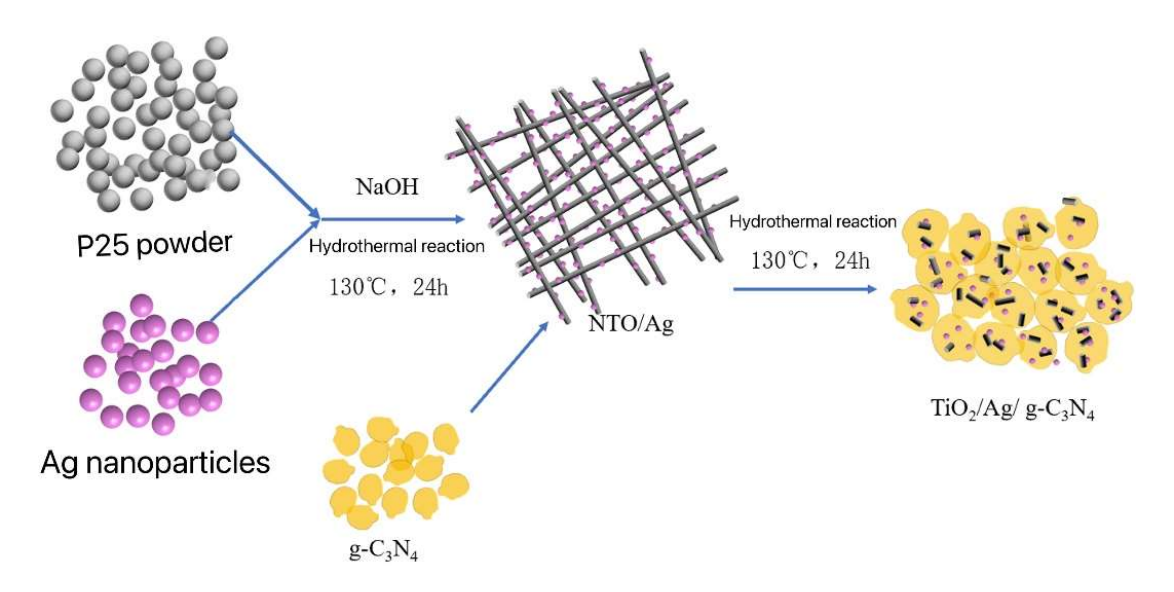
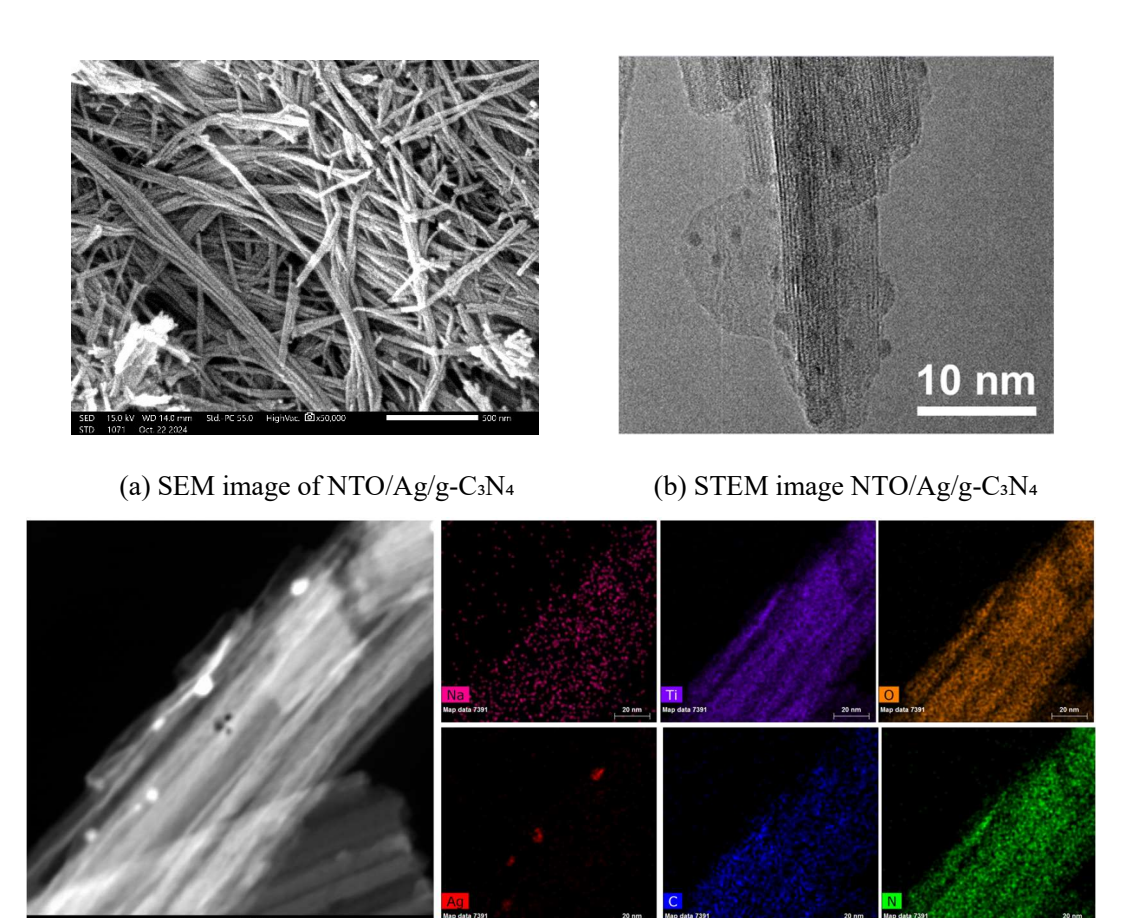


Fig. 3.5 Schematic illustration of preparation process of TiO₂/Ag/g-C₃N₄

The prepared NTO/Ag/g-C₃N₄ suspension and its morphology are shown as Fig. 3.6 and Fig. 3.7. The ternary composite catalyst obtained by the one-step hydrothermal reaction has an ultra-long nanowire structure with a length longer than 2 μm. It can be seen that the Ag nanoclusters distribute evenly on NTO nanowires and the g-C₃N₄ nanoplates attach on NTO nanowires. The EDS element mapping of NTO/Ag/g-C₃N₄ illustrates the presence of Na, Ti, O, Ag, C and N in the sample, which also confirms the formation of NTO and the composite of NTO, Ag and g-C₃N₄. The preparation of the NTO/Ag/g-C₃N₄ ternary composite material by adding Ag and g-C₃N₄ into P25 hydrothermal reaction system is shown in Fig. 3.8.



Fig. 3.6 NTO/Ag/g-C₃N₄ suspension by hydrothermal reaction



(c) HAADF-STEM and corresponding EDS elemental mapping images of NTO/Ag/g-C₃N₄

Fig. 3.7 SEM and STEM images of NTO/Ag/g-C₃N₄

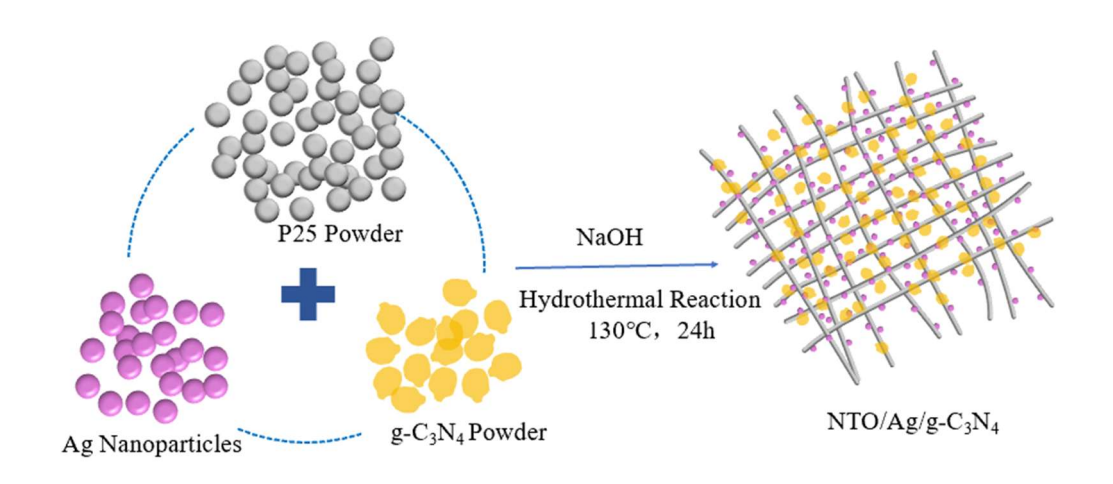


Fig. 3.8 Schematic illustration of preparation process of NTO/Ag/g-C₃N₄

Fig. 3.9 is the XRD patterns of the as-prepared NTO, NTO/Ag, TiO₂/Ag/g-C₃N₄, and NTO/Ag/g-C₃N₄ samples. For NTO, NTO/Ag and NTO/Ag/g-C₃N₄ samples, the characteristic diffraction peaks at 25.7°, 29.9° and 47.8° matches well with the

characteristic peaks of sodium titanate (JCPDS 31-1329), indicating that P25 has been successfully converted to NTO nanowires in an aqueous solution with high NaOH concentration. There are characteristic peaks at 38.2°, 44.2°, 64.4° and 77.1° in both NTO/Ag, TiO₂/Ag/g-C₃N₄ and NTO/Ag/g-C₃N₄ samples, which confirms the presence of Ag element. Characteristic peaks of g-C₃N₄ can be both observed in TiO₂/Ag/g-C₃N₄ and NTO/Ag/g-C₃N₄ catalysts. In the XRD patterns of TiO₂/Ag/g-C₃N₄ samples, beside the characteristic peaks of Ag, the characteristic peaks of TiO₂ (characteristic peaks at 25.7°、48.3°、54.3°、63.0°、69.2°、70.6° and 75.4°) can ben observed instead of NTO, which indicates that NTO has been converted to TiO₂ after hydrothermal reaction.

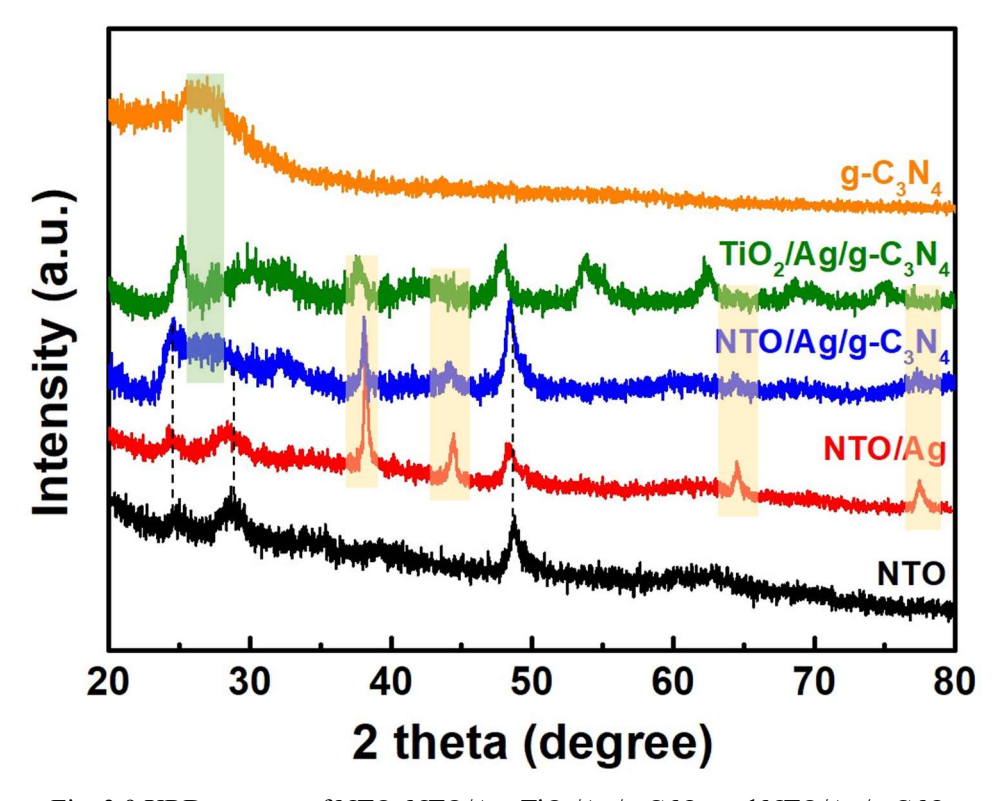


Fig. 3.9 XRD patterns of NTO, NTO/Ag, TiO₂/Ag/g-C₃N₄, and NTO/Ag/g-C₃N₄

3.2 Visible Light Absorption Analysis

Fig. 3.10 shows the UV-visible diffuse reflectance spectra of NTO, NTO/Ag, g- C_3N_4 , $TiO_2/Ag/g-C_3N_4$ and NTO/Ag/g- C_3N_4 . NTO only shows obvious absorption of ultraviolet light (λ < 400 nm) and little absorption of visible light. NTO/Ag, because of the addition of Ag nanoparticles, can not only absorb ultraviolet light, but also show

certain absorption of visible light in the wavelength range of 400-700 nm, among which the absorption capacity of visible light in the wavelength range of 400-500 nm is stronger, which may be due to the surface plasmon resonance effect of Ag nanoparticles resulting in strong absorption of visible light on the Ag surface. g-C₃N₄ shows strong absorption capacity for both ultraviolet light and visible light, especially for light with a wavelength of 250-600 nm.

The TiO₂/Ag/g-C₃N₄ and NTO/Ag/g-C₃N₄ ternary composites prepared by hydrothermal method in this study both show obvious absorption of visible light. Compared with pure NTO and NTO/Ag binary composite, the absorption capacity of ternary composites for ultraviolet light and visible light is improved, especially the absorption capacity of visible light in the wavelength range of 400-750 nm. It can be seen that the composite of NTO/Ag and semiconductor g-C₃N₄ can effectively improve the absorption capacity of the composite material for visible light, thereby improving its photocatalytic efficiency.

Comparing TiO₂/Ag/g-C₃N₄ and NTO/Ag/g-C₃N₄, NTO/Ag/g-C₃N₄ shows better light absorption capacity, which is mainly attributed to the special linear structure of NTO, which leads to a larger specific surface area and can increase the area of light absorption. At the same time, the surface of one-dimensional NTO contains more defect structures such as vacancies, which can serve as capture centers for photogenerated electron-hole pairs and improve light absorption efficiency.

Among all the catalyst systems prepared in this study, NTO/Ag/g- C_3N_4 exhibits the best visible light absorption capacity and excellent photoelectric properties. It can be predicted that it has the best photocatalytic performance and the ability to split water to produce hydrogen.

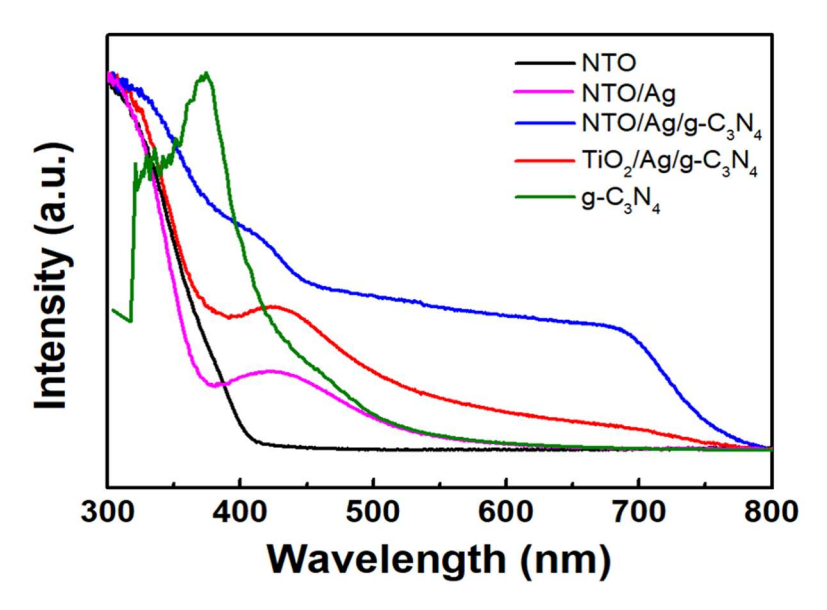


Fig. 3.10 UV-Vis Spectra of Various Photocatalysts

3.3 Membranes Fabrication

To maximize the specific surface area of the catalyst and thereby improve its catalytic efficiency, approximately 30 mg of TiO₂/Ag/g-C₃N₄ was initially subjected to suction filtration. However, the resulting catalyst membrane exhibited poor formability. Subsequently, the catalyst dosage was adjusted to ~60 mg for the follow-up experiment. As presented in Fig. 3.11, it is evident that for a suction filter flask with a diameter of 30 mm, 60 mg of TiO₂/Ag/g-C₃N₄ enables the fabrication of a well-shaped self-supporting membrane, with a thickness of approximately 1 mm. After the filtered TiO₂/Ag/g-C₃N₄ sample was dried in a vacuum drying oven for 12 h, the membrane showed distinct curling and cracking, which may be attributed to the nanorod microstructure of TiO₂/Ag/g-C₃N₄. The suction-filtrated TiO₂/Ag/g-C₃N₄ self-supporting membrane, formed by particle stacking, exhibits inadequate toughness post-drying, failing to retain its integral self-supporting configuration.





(a) $TiO_2/Ag/g$ - C_3N_4 membrane by suction filtration

(b) Dried TiO₂/Ag/g-C₃N₄ membrane

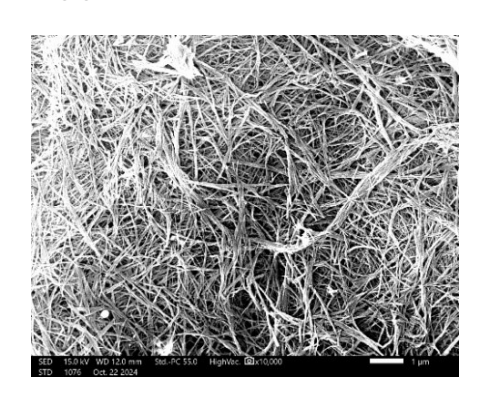
Fig. 3.11 Self-supporting TiO₂/Ag/g-C₃N₄ membrane

On the other hand, the membrane obtained by suction filtration from NTO/Ag/g-C₃N₄ suspension is shown in the Fig. 3.12. The sample surface has a fluffy structure like floc, which is presumed to be caused by the irregular entanglement of NTO nanowires. The suction-filtered NTO/Ag/g-C₃N₄ membrane was then subjected to liquid nitrogen freezing and transferred to a lyophilizer for 24 h of drying. As presented in Fig. 3.12(b), the final sample featured uniform thickness and intact morphology, with no warping or brittle fracture observed. Upon detachment from the filter paper, the sample remained free of tearing or damage—indicating strong interparticle bonding, adequate mechanical strength and toughness, and excellent retention of the selfsupporting membrane state. Fig. 3.12(c) shows the morphology of the NTO/Ag/g-C₃N₄ membrane surface, revealing a disordered, cross-linked nanowire structure. Fig. 3.12(d) shows the morphology of longitudinal section of the NTO/Ag/g-C₃N₄ membrane, demonstrating a multi-layered fibrous architecture along the thickness direction, which is attributed to the micrometer-scale length of the NTO nanowires. The NTO/Ag/g-C₃N₄ membrane is a multi-layered nanofiber membrane formed by the cross-linking of NTO ultra-long nanowires.





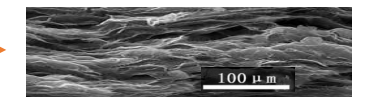
(a) NTO/Ag/g-C₃N₄ membrane afer suction-filtration (b) Dried NTO/Ag/g-C₃N₄ membrane





(c) Morphology of the surface of NTO/Ag/g-C $_3$ N $_4$ membrane





(d) Morphology of longitudinal section of the NTO/Ag/g-C₃N₄ membrane

Fig. 3.12 Morphology of the NTO/Ag/g-C₃N₄ membrane

3.4 Hydrogen Production by Photocatalytic Seawater Splitting

The quartz reactor with powder catalysts and catalysts membrane are shown as Fig. 3.13.



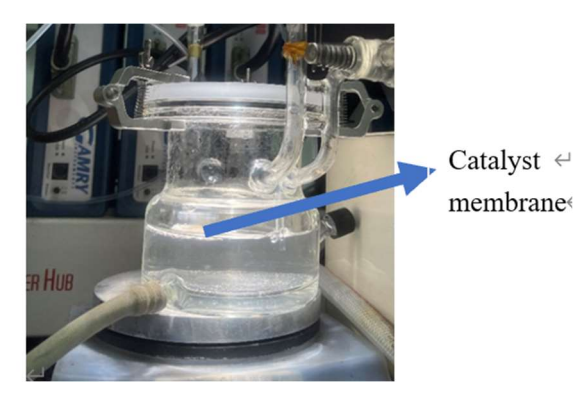


Fig. 3.13 Reactors with (a) Powder Catalyst and (b) Membrane Catalyst

No hydrogen production was detected when NTO and NTO/Ag were used as catalysts. This is primarily because of the weak visible-light absorption capacity of NTO. When Ag particles were used to modify NTO nanowires, the low loading amount of Ag resulted in only a limited improvement in the catalytic efficiency of NTO.

As can be seen from Fig. 3.14, hydrogen production was detected for all ternary composite catalysts, while the hydrogen production efficiency of powdered catalysts was generally higher than that of membrane catalysts. This is presumably because powdered catalysts dispersed uniformly and sufficiently in the simulated seawater and can achieve the best photocatalytic efficiency. For powdered catalysts, the hydrogen production amount showed an approximately linear increase with time. The hourly hydrogen production of TiO₂/Ag(2%)/g-C₃N₄ powder was about 365 μmol/g, while the catalytic hydrogen production efficiency of NTO/Ag(2%)/g-C₃N₄ was approximately 660 μmol/(g.h) - far higher than that of TiO₂/Ag(2%)/g-C₃N₄ powder. This may be attributed to the one-dimensional ultra-long nanowire structure of NTO, which is more conducive to the efficient separation and rapid transfer of photogenerated charge carriers.

When the NTO/Ag(2%)/g-C₃N₄ self-supporting membrane served as the catalyst, the hydrogen production reached ~225 µmol/g in the first hour, ~240 µmol/g in the second hour, and increased significantly to ~395 µmol/g in the third hour - far higher than the values in the preceding two hours - the catalyst's hydrogen production efficiency gradually improved with the extension of simulated seawater splitting time. This phenomenon is presumably ascribed to the gradual adsorption of seawater by the catalyst membrane during the reaction, which facilitates the participation of more catalytic active sites in seawater splitting for hydrogen production and thus contributes to the increased hydrogen output. Notably, the self-supporting membrane remained floating on the surface of simulated seawater throughout the reaction due to its low density, preventing the surface-layer catalysts from engaging in the reaction. For

subsequent experiments, reducing the thickness of the catalyst membrane and exploring special measures to ensure its complete immersion in simulated seawater are recommended to enhance the utilization efficiency of the catalyst membrane.

The catalytic performance of NTO/Ag(5%)/g-C₃N₄ is significantly better than that of the NTO/Ag(2%)/g-C₃N₄, while the cumulative hydrogen production amounts at 1h, 2h, and 3h reached 858.6, 2161.5, and 3504 µmol/g, respectively. This is mainly because the addition of Ag ions is beneficial to the separation of photogenerated carriers in NTO, reduces the recombination of surface photogenerated electrons and holes, and enables more electrons and holes to participate in the redox reaction. Ag ions can also improve the visible light absorption ability of NTO, thereby enhancing its photocatalytic activity.

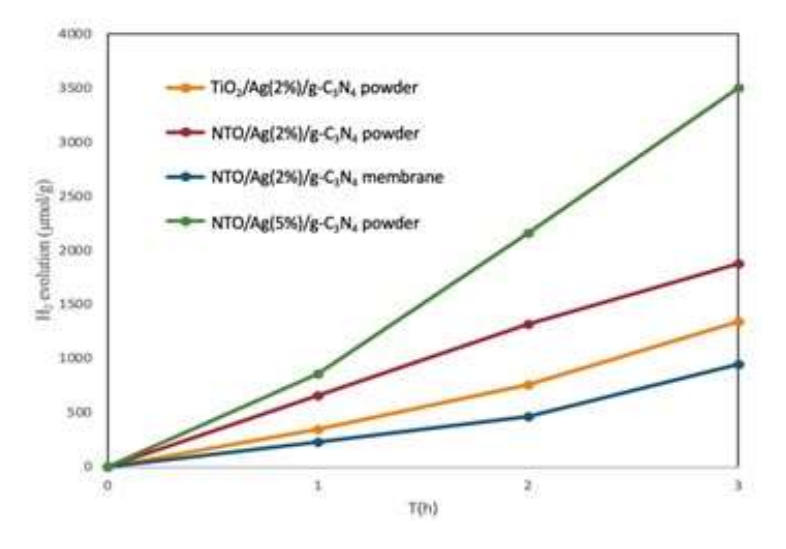


Fig. 3.14 Hydrogen production efficiencies of TiO₂/Ag/g-C₃N₄ and NTO/Ag/g-C₃N₄

Obviously, the powdered catalyst dispersed in seawater is difficult to recover after the reaction, which may cause pollution to seawater (Fig. 3.13(a)). As shown in Fig. 3.15, the self-supporting membrane still maintains good shapes after 3 h reaction, and the simulated seawater remains clean without suspended particles, which means the membrane can be easily recycled and reused, and will not cause additional pollution to the seawater.



Fig. 3.15 NTO/Ag/g-C₃N₄ membrane after a 3-h reaction

3.5 Mechanism of NTO/Ag/g-C₃N₄ for photocatalytic Hydrogen Production

A Z-scheme heterojunction mechanism for NTO/Ag/g-C₃N₄ is proposed, as Fig. 3.16. The remarkable enhancement in the photocatalytic performance of the ternary NTO/Ag/g-C₃N₄ composite can be attributed to two primary factors. First, upon visible light irradiation, the exposed Ag nanoclusters anchored on the NTO surface are excited to generate hot electrons and holes. The photoexcited electrons are injected into the conduction band (CB) of NTO, whereas the photogenerated holes are captured by the sacrificial agent. Notably, the energy transfer derived from the plasmonic effect substantially elevates the carrier concentration of NTO. Second, the Ag nanoparticles which are in contact with both g-C₃N₄ and NTO also function as an electronic mediator between the valence band (VB) of g-C₃N₄ and the CB of NTO. This interfacial electron transfer behavior facilitates the formation of a Z-scheme heterojunction, thereby conferring the composite with high photocatalytic activity toward H⁺ reduction. Furthermore, the cyclic transformation of Cl⁻-Cl₂-HClO⁻-Cl⁻ involving Cl⁻ ions in simulated seawater effectively promotes the separation of photogenerated electron-hole pairs, which further enhances the overall photocatalytic activity.

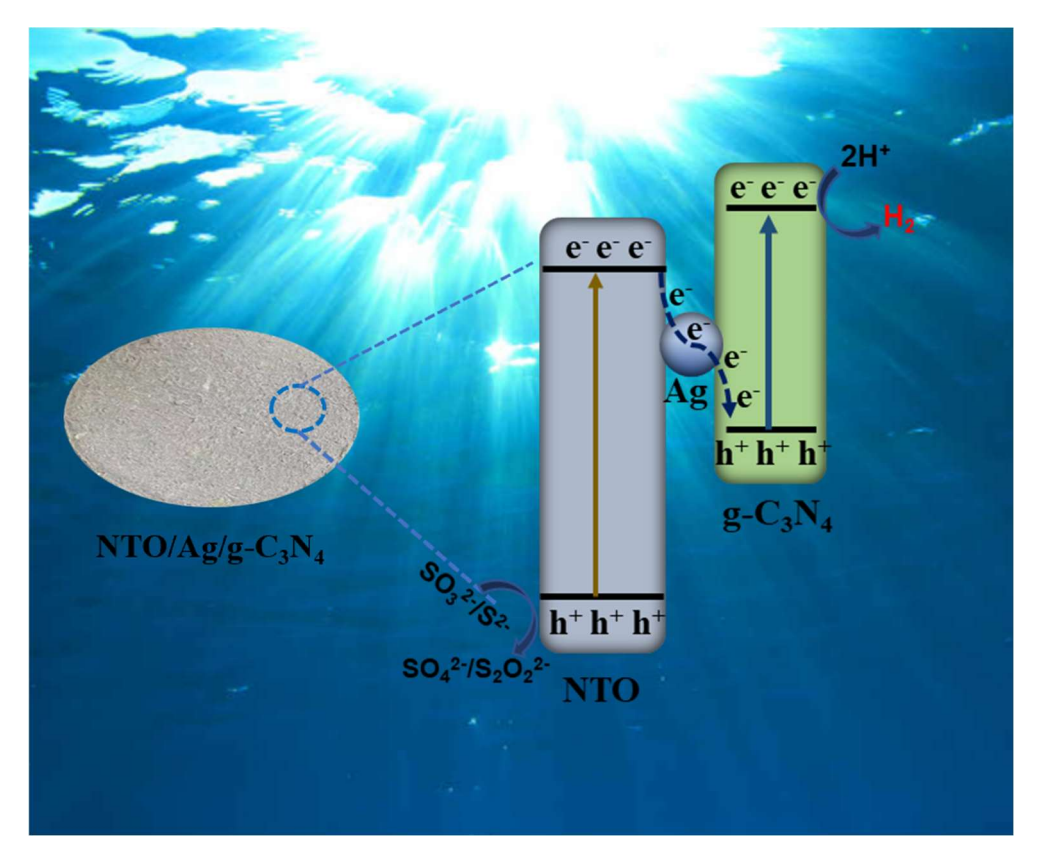


Fig. 3.16 Schemetic illustration of the charge transfer in NTO/Ag/g-C₃N₄ for photocatalytic H_2 evolution

4. Conclusions and Outlooks

4.1 Conclusions

Two kinds of ternary composite photocatalysts, TiO₂/Ag/g-C₃N₄ and NTO/Ag/g-C₃N₄, were synthesized respectively by two-step of hydrothermal reactions and one-step hydrothermal reactions. Both the visible-light absorption capability and photocatalytic hydrogen evolution performance of NTO/Ag/g-C₃N₄ are significantly superior to those of TiO₂/Ag/g-C₃N₄ because of the ultra-long nanowire architecture of NTO, which enables more efficient separation and rapid transfer of photogenerated carriers.

A Z-scheme heterojunction configuration for NTO/Ag/g-C₃N₄ is proposed. The Ag nanoparticles anchored on the surface of NTO nanowires serve dual functions: first, they act as an electronic mediator to facilitate the formation of the Z-scheme heterojunction, which promotes the effective separation of electron-hole pairs; second, they generate hot electrons that further boost the progression of the photocatalytic reaction. Moreover, the synergistic interaction between g-C₃N₄ nanosheets and Ag nanoclusters remarkably broadens the visible-light absorption range and enhances the absorption intensity of the photocatalyst. Experimental results further demonstrate that increasing the Ag content contributes to the improvement of the photocatalytic performance of NTO/Ag/g-C₃N₄. Specifically, the hydrogen evolution rate of NTO/Ag(5%)/g-C₃N₄ is much higher than that of NTO/Ag(2%)/g-C₃N₄, with a maximum value of 1168 µmol/(g·h).

Leveraging the ultra-long nanowires of NTO, a shape-stable self-supporting NTO/Ag/g-C₃N₄ membrane was successfully fabricated through suction filtration followed by freeze-drying. After a continuous reaction with simulated seawater for 3 h, the membrane retained its original morphology without leaving any residues in the seawater, thus preventing potential contamination. This study is anticipated to provide valuable insights for the design of high-efficiency and stable Z-scheme photocatalysts applicable to visible-light-driven seawater splitting for hydrogen production.

4.2 Outlooks

- 1. The ternary composite catalyst synthesized via the hydrothermal method in this study exhibits low production efficiency, which is significantly inconsistent with practical requirements. Thus, further exploration of synthetic methodologies is imperative to effectively enhance the production efficiency of the catalyst.
- 2. The thickness of the self-supporting membrane exerts a significant influence on its catalytic efficiency: a smaller membrane thickness corresponds to a larger specific surface area, thereby resulting in higher catalytic efficiency. However, the vacuum suction filtration method employed in this study poses challenges to the precise control of membrane thickness, necessitating further investigation into optimized membrane fabrication strategies.

References

- [1] Fujishima A, Honda K. Electrochemical photolysis of water at a semiconductor electrode [J]. Nature. 1972, 238(5358): 37-38.
- [2] https://www.eenewseurope.com/en/submersible-solar-cell-promises-water-splitting-renewable-fuel-generation/
- [3] Zhu S, Wang D. Photocatalysis: basic principles, diverse forms of implementations and emerging scientific opportunities [J]. Adv Energy Mater. 2017, 7(23): 1700841.
- [4] Qian R, Zong H, Schneider J, et al. Charge carrier trapping, recombination and transfer during TiO₂ photocatalysis: An overview [J]. Catal Today. 2019, 335: 78-90.
- [5] Hu H, Lin Y, Hu Y H. Synthesis, structures and applications of single component core-shell structured TiO₂: A review [J]. Chem Eng J. 2019, 375: 122029.
- [6] Yoshida T, Misu Y, Yamamoto M, et al. Effects of the amount of Au nanoparticles on the visible light response of TiO₂ photocatalysts [J]. Catal Today. 2020, 352: 34-38.
- [7] Zhang Y, Jiang Z, Huang J, et al. Titanate and titania nanostructured materials for environmental and energy applications: a review [J]. RSC Adv. 2015, 5(97): 79479-79510.
- [8] Lu S, Wang Y, Zhou Y, et al. Oxygen vacancy stimulated direct Z-scheme of mesoporous Cu₂O/TiO₂ for enhanced photocatalytic hydrogen production from water and seawater [J]. Journal of Alloys and Compounds, 2021,868:159144.
- [9] Veziroglu S, Obermann A L, Ullrich M, et al. Photodeposition of Au nanoclusters for enhanced photocatalytic dye degradation over TiO₂ thin film [J]. ACS Appl Mater Inter. 2020, 12(13): 14983-14992.
- [10] Zhang W, He H, Li H, et al. Visible-light responsive TiO₂-based materials for efficient solar energy utilization [J]. Adv Energy Mater. 2020, 11(15): 2003303.
- [11] Prakash J, Sun S, Swart H C, et al. Noble metals-TiO₂ nanocomposites: from fundamental mechanisms to photocatalysis, surface enhanced Raman scattering and antibacterial applications [J]. Appl Mater Today. 2018, 11: 82-135.
- [12] Park H, Park Y, Kim W, et al. Surface modification of TiO₂ photocatalyst for environmental applications [J]. J Photoch Photobio C. 2013, 15: 1-20.

- [13] Liu X, Ye M, Zhang S, et al. Enhanced photocatalytic CO₂ valorization over TiO₂ hollow microspheres by synergetic surface tailoring and Au decoration [J]. J Mater Chem A. 2018, 6(47): 24245-24255.
- [14] Dong W, Xiao Y X, Yang K R, et al. Pt nanoclusters on GaN nanowires for solar-assisted seawater hydrogen evolution [J]. Nat Commun. 2023, 14(179): 62-85.
- [15] Lee W H, Lee C W, Cha, G D, et al. Floatable photocatalytic hydrogel nanocomposites for large-scale solar hydrogen production [J]. Nat Nanotechnol. 2023, 18: 754–762.
- [16] Li Y, Zhang L, et al. Recent Progress in TiO₂ nanostructures for efficient solar-driven water splitting [J]. Adv Mater. 2022, 34(17), 2108223.
- [17] Guo X., Liu X., et al. Heterojunction design between WSe2 nanosheets and TiO₂ for efficient photocatalytic hydrogen generation [J]. Catalysts. 2022, 12(12), 1668.
- [18] Wang S, Yun JH, Luo B, et al. Recent progress on visible light responsive heterojunctions for photocatalytic applications [J]. J Mater Sci Technol. 2017, 33(1): 1-22.
- [19] Low J, Yu J, Jaroniec M, et al. Heterojunction photocatalysts [J]. Adv Mater, 2017, 29(20): 1601694.
- [20] Jing X C, Sun Z H, Yin H, et al. Metamaterial-enhanced solar-driven processes for energyconversion and water treatment [J]. Adv Sci. 2025, e08046.

https://doi.org/10.1002/advs.202508046

- [21] Li J T, Cushing S K, Zhang P, et al. Solar hydrogen generation by a CdS-Au-TiO₂ sandwich nanorod array enhanced with Au nanoparticle as electron relay and plasmonic photosensitizer [J]. J Am Chem Soc, 2014, 136(23): 8438–8449.
- [22] Luo F, Liao S, Dang D, et al. Tin and silicon binary oxide on the carbon support of a Pt electrocatalyst with enhanced activity and durability. ACS Catal. 2015, 5(4): 2242.
- [23] Wang Y, Cao Q, Guan C, Cheng C. Recent advances on self-supported arrayed bifunctional oxygen electrocatalysts for flexible solid-state Zn–air Batteries. Small 2020, 16(33): 2002902.
- [24] Wang P, Jia T, Wang B. A critical review: 1D/2D nanostructured self-supported

electrodes for electrochemical water splitting Power Sources 2020, 474: 228621.

[25] López Zavala M Á, Lozano Morales S A, Ávila-Santos Manue. Synthesis of stable TiO₂ nanotubes: effect of hydrothermal treatment, acid washing and annealing temperature. Heliyon, 2017, 3(11): e00456

Acknowledgements

This research project was completed under the meticulous guidance of my supervisor, Professor Weihong Zhu. I would like to express my sincere gratitude to Professor Zhu for guiding me to the realm of science. For the research topic, Professor Zhu not only fully respected my interests but also provided crucial and timely guidance and suggestions on specific research orientations. Prof. Zhu's group fosters an exceptionally positive academic atmosphere, from which I have benefited tremendously.

I would also like to thank Professor Zhiqian Guo of the research group for his dedicated guidance on experimental directions and research routes, as well as Ms. Juan Li for her guidance and assistance in instrument operation and daily administrative affairs.

My gratitude extends to Senior Fellow Yu Chu for his meticulous guidance at the initial stage of my experiments. From laboratory safety to the operation of various instruments and the preparation of chemical reagents, Senior Chu patiently guided me through the fundamentals. I am equally thankful to Senior Fellow Yufeng Yin for her companionship and guidance throughout the experimental process. Given the wide variety of reagents used in this project, the long reaction durations, and the complexity of the experiments—coupled with the need to balance academic studies at school—I deeply appreciate the assistance provided by Senior Fellow Yin over the past 12 months. Her support enabled me to promptly monitor the progress of experiments and adjust or continue experimental protocols as needed. I would also like to thank Senior Fellow Xuecong Pan for helping me set up the hydrogen production experimental system on each occasion. Due to the long duration of hydrogen production reactions, each experiment—from system setup to completion—required at least four hours, and on several occasions extended past 1:00 a.m. I am extremely grateful for Senior Fellow Pan's guidance and companionship throughout these processes. Additionally, I would like to acknowledge the selfless guidance and support from Senior Fellows Chu, Yin, and Pan in experimental data processing and academic paper writing.

Finally, I want to express my thanks to my alma mater, Shanghai Foreign Language School Affiliated to Shanghai International Studies University. Committed to promoting the diversified development of students under the immersion of multiculturalism, the school has provided students with a variety of platforms for scientific and technological innovation. I would like to thank Qixiang Li and Mr. Shuhong Min for their extensive guidance and assistance in my chemistry studies, as well as Ms. Rongqin Yan and Mr. Haobin Zhu for their support in scientific and technological innovation activities. My gratitude also goes to my homeroom teacher, Ms. Zhe Zhang.